Observations of the 14 July 2011 Fort Collins Hailstorm: Implications for WSR-88D-Based Hail Detection and Warnings

PATRICK C. KENNEDY, STEVEN A. RUTLEDGE, AND BRENDA DOLAN

Department of Atmospheric Science, Colorado State University, Fort Collins, Colorado

ERIC THALER

NOAA/National Weather Service Forecast Office, Denver/Boulder, Denver, Colorado

(Manuscript received 28 June 2013, in final form 13 February 2014)

ABSTRACT

The issuance of timely warnings for the occurrence of severe-class hail (hailstone diameters of 2.5 cm or larger) remains an ongoing challenge for operational forecasters. This study examines the application of two remotely sensed data sources between 0100 and 0400 UTC 14 July 2011 when pulse-type severe thunderstorms occurred in the jurisdiction of the Denver/Boulder National Weather Service (NWS) Forecast Office in Colorado. First, a developing hailstorm was jointly observed by the dual-polarization Colorado State University–University of Chicago–Illinois State Water Survey (CSU–CHILL) research radar and by the operational, single-polarization NWS radar at Denver/Front Range (KFTG). During the time period leading up to the issuance of the initial severe thunderstorm warning, the dual-polarization radar data near the 0 °C altitude contained a positive differential reflectivity Z_{DR} column (indicating a strong updraft lofting supercooled raindrops above the freezing level). Correlation coefficient ρ_{HV} reductions to ~0.93, probably due to the presence of growing hailstones, were observed above the freezing level in portions of the developing >55-dBZ echo core. Second, data from the National Lightning Detection Network (NLDN), including the locations and polarity of cloud-to-ground (CG) discharges produced by several of the evening's storms, were processed. Some association was found between the prevalence of positive CGs and storms that produced severe hail. The analyses indicate that the use of the dual-polarization data provided by the upgraded Weather Surveillance Radar-1988 Doppler (WSR-88D), in combination with the NLDN data stream, can assist operational forecasters in the real-time identification of thunderstorms that pose a severe hail threat.

1. Introduction

The National Weather Service (NWS) recently upgraded its Weather Surveillance Radar-1988 Doppler (WSR-88D) network to collect dual-linear-polarization data. This upgrade was done in recognition of the information on the mean hydrometeor shape and orientation characteristics that can be extracted from the horizontally H and vertically V polarized received signal components. Two polarimetric measurements that are useful for the differentiation of hailstones from raindrops are the H/V ratio of the received signal amplitudes (differential reflectivity Z_{DR}), and the degree of correlation between the amplitudes and phases of the H and V returns ρ_{HV}. Hailstones typically gyrate through large (~45° or more) orientation angles as they fall (Knight and Knight 1970). In contrast, the balance of the aerodynamic and internal fluid forces acting on raindrops with diameters larger than ~1 mm produces an oblate equilibrium shape. The chaotic hailstone orientations tend to equalize the H and V received signal powers, while the oblate raindrop shapes preferentially increase the H received power relative to the V received power. Thus, to a first approximation, decreased Z_{DR} magnitudes in high-reflectivity thunderstorm echo cores imply the presence of hail (Aydin et al. 1986). The correlation coefficient between the H and V return signals is decreased as the spectrum of hydrometeor compositions (i.e., ice vs liquid), shapes, and orientations increases within the radar pulse volume (Balakrishnan and Zrnić 1990; Kumjian et al. 2010).

Corresponding author address: Patrick C. Kennedy, CSU-CHILL Radar, 30750 Weld County Road 45, Greeley, CO 80631.
E-mail: patrick.kennedy@colostate.edu

DOI: 10.1175/WAF-D-13-00075.1

The storms analyzed in this study occurred in July 2011, before the dual-polarization upgrade had been completed on the WSR-88D radars that cover northern Colorado. Polarimetric observations were made by the Colorado State University–University of Chicago–Illinois State Water Survey (CSU-CHILL) radar. Because CSU-CHILL operates at S band like WSR-88D, the observed dual-polarization patterns should be similar to those that have become available with the upgraded NWS radars. In addition to dual-polarization hail signatures, the polarity characteristics of cloud-to-ground (CG) lightning detected by the National Lightning Detection Network (NLDN) during the analysis period are also examined. The objective of this work is the documentation of the evolution of key dual-polarization radar parameters and NLDN CG polarity trends during the time period when the decision to issue a severe thunderstorm warning due to the expectation of large hail was being made.

a. Synoptic setting

During 0000–0400 UTC 14 July 2011 [1800–2200 mountain daylight time (MDT) 13 July 2011] multiple severe thunderstorms produced damaging hail and local flash flooding across a region encompassing the greater Denver–Fort Collins area of northern Colorado. In chronological order, the primary events were (i) 2.5–3.8 cm (1.0–1.5 in.)–diameter hail over the western portions of the Denver area between 0010 and 0040 UTC, (ii) flash flooding in the burn scar area of the Fourmile Canyon fire (which started on 6 September 2010 and burned 6181 acres) in Boulder County near 0100 UTC, (iii) 2.5–4.4 cm (1.0–1.75 in.)–diameter hail along a swath from near the city of Lyons to southern Fort Collins between 0111 and 0152 UTC, and (iv) 2.5 cm (1.0 in.)–diameter hail and 25 m s^{-1} (51 knots; kt; 1 kt = 0.51 m s^{-1}) winds observed at Denver International Airport, resulting in significant damage to parked aircraft around 0330 UTC. The main focus of this study is the Fort Collins hailstorm, the third event in this sequence.

This series of severe weather events took place while a deep southwesterly monsoonal flow pattern (Higgins et al. 1997) was established over the southwestern United States. Storm initiation took place over the foothills of the Rocky Mountains in the greater Denver area. The Denver radiosonde observation at 0000 UTC 14 July showed that appreciable moisture was present between the top of the boundary layer and the 280-hPa level; the sounding's precipitable water and convective available potential energy (CAPE) values were 2.82 cm (1.1 in.) and 950 J Kg^{-1}, respectively (Fig. 1). Wind speeds were modest (20 m s^{-1} or less) at all levels. The wind direction initially backed from 130° at the surface to 095° at 1526 m AGL. (i.e., the shear vector turned counterclockwise with height through the first 1.5 km). Above this level, the wind veered to ~240° at 3 km AGL; this general direction was then maintained throughout the remainder of the sounding. The magnitude of the 0–6 km AGL wind vector difference was 13.8 m s^{-1}. These instability and wind shear magnitudes were conducive to the development of shorter-lived, nonsupercell thunderstorms (Rasmussen and Blanchard 1998).

b. Radar observations

The NWS radar at Denver (KFTG) was still configured in single-polarization mode in July 2011. (The dual-polarization upgrade was completed in September 2012.) Due to the thunderstorm activity, KFTG was operating in severe weather mode [volume coverage pattern (VCP) 12] with scan update times of ~4 min during the analysis period.

The CSU-CHILL research radar is located ~75 km north of KFTG near Greeley, Colorado. Like KFTG, CSU-CHILL operates in the 10–11-cm-wavelength S band and has an antenna main beam pattern width of ~1°. During this event the transmit polarization was being alternated on a pulse-to-pulse basis, allowing measurement of the same basic dual-polarization variables that are output by the upgraded WSR-88D systems. (The alternating-polarization mode also allows CSU-CHILL to measure the linear-depolarization ratio L_{DR}; the upgraded WSR-88D systems simultaneously radiate unmodulated *H*- and *V*-polarized waves, preventing the measurement of L_{DR}). CSU-CHILL operations were being done for a research project investigating the evolution of convective rainfall intensities over the foothills of the Rocky Mountains and the higher population density area in the plains immediately to the east of the foothills (Matrosov et al. 2013). To support this project, the CSU-CHILL scan pattern consisted of plan position indicator (PPI) sector sweeps covering the general Denver region northward to the Fort Collins area. These sweeps were executed at eight elevation angles between 0.5° and 10°. Range–height indicator (RHI) scans were interspersed through the most intense echo cores. The overall scan cycle time was ~4.5 min. No special efforts were made to bring the CSU-CHILL volume scan starting times into synchronization with those of KFTG.

2. Hail indications in 11-cm-wavelength dual-polarization radar data

When using dual-polarization-radar data to diagnose the presence of hail, training materials prepared by the NWS Warning Decision Training Branch (WDTB) advise operational forecasters to primarily examine the

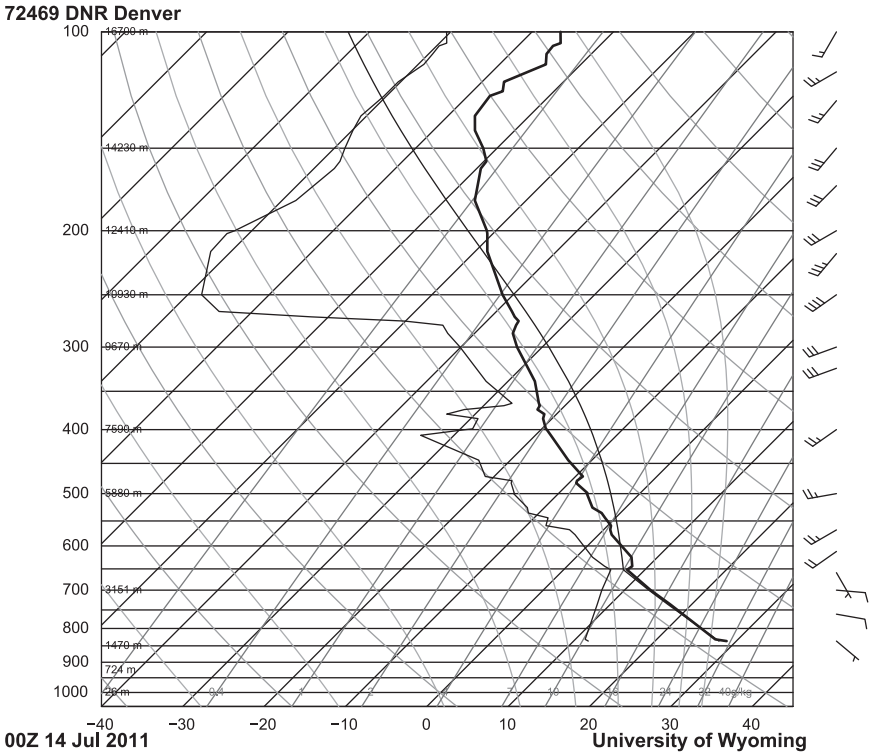

FIG. 1. Skew T–log$p$ plot of the Denver radiosonde data at 0000 UTC 14 Jul 2011 from the University of Wyoming archives with wind barbs (kt). CAPE is 950 J kg^{-1} based on virtual temperature and a surface-layer mixing depth of 500 m. Precipitable water is 2.82 cm (1.1 in.).

copolar correlation coefficient (ρ_{HV}) and differential reflectivity (Z_{DR}) fields in relationship to thunderstorm structural features evidenced by conventional reflectivity Z_H and radial velocity patterns. The following brief summaries are provided to aid in the interpretation of the S-band polarimetric variables relevant to operational hail detection.

The copolar correlation coefficient (ρ_{HV}) is an expression of the combined phase and amplitude correlation between the H and V returns received from each sample volume during a signal integration cycle (typically ~40 pulses for the WSR-88D and ~100 pulses for CSU-CHILL). The ρ_{HV} values approach unity when the radar sample volume contains a relatively homogenous collection of hydrometeor types, shapes, and orientations. For example, in well-sampled rain (signal to noise ratio >5 dB), ρ_{HV} typically reaches levels of ~0.98 or higher at S band. The shape and orientation variations of hailstones tend to decrease the correlation between the individual H and V signal returns. This effect is magnified when hailstones and raindrops coexist in the sample volume and produce a wider variety of hydrometeor forms and alignments (Balakrishnan and Zrnić 1990). Due to these effects, ρ_{HV} is generally reduced to 0.95 or less when significant concentrations of hailstones exist. More significant ρ_{HV} reductions can occur if the hailstone diameters become large enough to enter the Mie scattering regime. These effects become significant when the following ratio involving particle diameter and radar wavelength becomes approximately equal to unity (Kumjian and Ryzhkov 2008):

$$(D|\varepsilon|^{1/2})/\lambda\,, \tag{1}$$

where D is the hydrometeor equivolume sphere diameter (cm); $|\varepsilon|$ is the modulus of the unitless complex index of refraction value appropriate for the hydrometeor thermodynamic phase, temperature, and radar wavelength; and λ is the radar wavelength (cm).

For a solid-ice hailstone (i.e., without density-reducing air cavities or a liquid water component) at a temperature of 0°C and a 10-cm radar wavelength, this ratio become one at a diameter of 5.6 cm (~2 in.). The WDTB WSR-88D dual-polarization upgrade training materials indicate that hail in this "giant" diameter range is associated with ρ_{HV} reductions significantly below the range associated with most precipitation, in some cases below ~0.85 (Picca and Ryzhkov 2012).

Differential reflectivity (Z_{DR}) is the ratio of the copolar H and V reflectivities expressed on a logarithmic scale:

$$Z_{DR} = 10 \log_{10}(Z_{hh}/Z_{vv}), \quad (2)$$

where Z_{hh} and Z_{vv} are the copolar linear scale reflectivity values ($mm^6 m^{-3}$) at horizontal and vertical polarization (where the two letters hh or vv represent the receive and transmit signal polarizations), respectively.

The preferential horizontal orientation of raindrops causes the backscattering cross section for H-polarized waves to exceed that for V waves. The resultant Z_{hh}/Z_{vv} ratio in the argument of the logarithm in Eq. (2) is >1, yielding positive Z_{DR} values. (Observed Z_{DR} levels in rain are typically ~0.5–3.5 dB.) The tumbling motions of hailstones tend to equalize Z_{hh} and Z_{vv}, reducing Z_{DR} toward (and sometimes below) 0 dB (Herzegh and Jameson 1992). Melting ice particles in the small hail–graupel diameter range (smaller than ~1 cm) develop a torus of water centered near their equator (Rasmussen and Heymsfield 1987). The presence of this water stabilizes the tumbling motions and promotes positive Z_{DR} values than can exceed those expected from large raindrops. For radar wavelengths of 10–11 cm, "classic" hailstones (i.e., stones whose gyrating motions are not being stabilized by surface meltwater accumulations) are typically characterized by relatively low (approaching 0 dB) Z_{DR} values and reduced (less than ~0.95)-ρ_{HV} magnitudes.

The relative phases of the horizontally and vertically polarized waves are also affected when hydrometeors with preferential orientations exist along the beam path. This differential propagation phase shift ϕ_{DP} arises due to the addition of the time-lagged forward-scattering components emitted by the individual hydrometeors to the microwave fields originally transmitted by the radar. For raindrops, the magnitude of this forward-scattering-induced phase lag is proportional to both the drop concentration and the drop oblateness (Jameson 1985). The derivative of ϕ_{DP} with respect to range (two-way specific-propagation differential phase K_{DP}) becomes more positive as the concentration of oblate hydrometeors along the radar beam path increases. Positive K_{DP} regions that extend up to subfreezing temperature levels in thunderstorm updrafts suggest the presence of significant concentrations of millimeter-sized, oblate hydrometeors, typically composed of mixed-phase particles and/or liquid drops (Kumjian and Ryzhkov 2008). The supercooled liquid component in positive K_{DP} columns can provide a favorable environment for enhanced hailstone growth rates.

3. CSU-CHILL and NWS WSR-88D observations of the Fort Collins hailstorm

As noted in the introduction, this study is primarily concerned with examining the development of hail-related polarimetric radar signatures at key points in the lifetime of the severe thunderstorm that affected the Lyons–Fort Collins area (hereafter termed the FCL storm) on the evening of 13 July 2011 (local date; i.e., the third event in the sequence given in the introduction). The reflectivity maximum associated with the FCL hailstorm began to split from the northern flank of the Fourmile Canyon echo complex (event two in the introduction sequence) at approximately 0045 UTC. The NWS Denver/Boulder Weather Forecast Office (WFO) issued the initial severe thunderstorm warning for the storm at 0113 UTC with the expectation of 2.5 cm (1 in.)–diameter hail. (At 0111 UTC a spotter report of 2.5-cm-diameter hail had been received.) The archived KFTG data from this general time period were replayed after the event at the Denver/Boulder WFO. It was determined that the characteristics of the storm as depicted in the WSR-88D displays probably began to attract heightened forecaster interest during the volume scan that began at 0104 UTC. The warning issuance decision was strongly influenced by the confirmatory/increasing severe thunderstorm characteristics [maximum reflectivity point value reaching 67 dBZ, vertically integrated liquid (VIL; Amburn and Wolf 1997) of 50–55 kg m^{-2}, and an increasingly well-defined three-body scattering spike (TBSS; Wilson and Reum 1988; Lemon 1998; Zrnić et al. 2010)] that were evident as the next (0109 UTC) volume scan progressed.

a. *Combined dual-Doppler and dual-polarization observations during the prewarning period*

Fortuitously, the KFTG and CSU-CHILL radars began volume scans with 30 s of each other on two occasions within the 10-min period prior to the issuance of the severe thunderstorm warning. This circumstance allowed the three-dimensional airflow within the developing storm at 0100 and 0110 UTC to be synthesized using dual-Doppler data-processing techniques. To support this processing, the data from each radar were interpolated to a common Cartesian gridpoint array (mesh size of 0.5 km in X, Y, and Z) using the National Center for Atmospheric Research (NCAR) Sorted Position Radar Interpolation (SPRINT; Mohr and Vaughn 1979) software. Wind field syntheses based on the gridded radial velocity input data were done using Custom Editing and Display of Reduced Information in Cartesian space (CEDRIC; Mohr et al. 1986) routines.

Because the rainfall mapping project's scanning restricted the maximum elevation angle scanned by the

CSU-CHILL radar to 10°, sampling of the divergent flow in the anvil levels of the storm at heights above ~10.5 km MSL was incomplete. As a result, vertical air motions were calculated by integrating the horizontal divergence fields in an upward direction. At the lower levels, ground clutter returns from the foothills of the Rocky Mountains raised the lowest usable analysis height to 2.5 km MSL, so the convergence/divergence patterns near the surface were not well represented either. Due to these limitations, it is roughly estimated that midlevel vertical velocities have uncertainties as large as 5–8 m s^{-1}; in this analysis emphasis is primarily placed on qualitative features.

Figure 2 shows dual-Doppler results at the 6 km MSL height level (environmental temperature of ~−7°C) obtained at 0100 and 0110 UTC. Based on the tracking of midlevel reflectivity features, a storm motion from 218° at 12 m s^{-1} was removed from the horizontal wind vectors. At the first analysis time, concerns that the storm would reach warning issuance criteria were starting to develop. Much of the echo core region with reflectivity levels above 55 dBZ was associated with updrafts greater than ~10 m s^{-1} (Fig. 2a). Anticyclonic vorticity encompassed most of the updraft area at this height level. As noted in section 4, the FCL hailstorm split from the left side of the Fourmile Canyon storm echo complex. The numerical simulations of Rotunno and Klemp (1982) have documented the tendency for anticyclonic rotation to develop in the left-moving member of splitting storms when the shear vector of the environmental winds rotates in a counterclockwise sense with increasing height. This shear vector variation was observed in the lowest 1.5 km of the Denver, Colorado (DNR), sounding. A region of reduced-ρ_{HV} magnitudes that included much of the updraft area also extended northward toward the leading edge of the storm (Fig. 2b). The supercooled liquid flux provided by the updraft apparently promoted vigorous hydrometeor growth in this area. The subfreezing temperatures and high-reflectivity levels imply a high likelihood that some of these hydrometeors were hailstones. The coexistence of hail with smaller raindrops and graupel particles growing within or carried aloft by the updraft would lead to localized ρ_{HV} reductions. The correspondence between the locations of the primary updraft and reduced-ρ_{HV} values is in agreement with the patterns noted in supercell storms by Kumjian et al. (2010).

The positive features in the Z_{DR} and K_{DP} field patterns indicate that oblate particles existed in the storm-relative inflow along the northwestern (left) flank of the updraft, with the positive K_{DP} contours occupying a relatively small horizontal area (Fig. 2c). A closer examination of the polarimetric data confirmed that both the K_{DP} and Z_{DR} maxima were continuous columnar structures that originated at lower/warmer temperature levels and extended upward into the subfreezing portion of the storm. The Z_{DR} columns have been associated with updrafts that are removed by vertically advecting the smaller (less than ~2-mm diameter), lower fall speed portion of the particle size distribution (Kumjian and Ryzhkov 2012). The remaining large, oblate drops and liquid-coated ice particles produce positive Z_{DR} values (Brandes et al. 1995; Loney et al. 2002). The enhanced values in the K_{DP} column have been related to mixed-phase hydrometeors and/or raindrops occurring in high concentrations (Loney et al. 2002). The positive K_{DP} magnitudes observed in this case were generally under 1° km^{-1}, less than the 1°–2° km^{-1} magnitudes reported in supercell storms (Kumjian and Ryzhkov 2008; Kumjian et al. 2010).

The second dual-Doppler synthesis opportunity occurred 10 min later (0110 UTC) and coincided with the initial issuance of the severe thunderstorm warning. The reflectivity core area, intensity, and associated updraft strength had all increased since the previous analysis time (Fig. 2d). The overall reflectivity pattern also began to display a three-body scattering echo extension ($X = -63$, $Y = -18$ km). The ρ_{HV} field contained a well-defined minimum within the strengthening updraft, with even lower ρ_{HV} values (0.88–0.92) near the junction of the three-body scattering and main storm echoes ($X = -60$, $Y = -17$ km; Fig. 2e; ρ_{HV} values below 0.6 were not recorded due to a signal processor threshold, which limits the three-body echo in Fig. 2e). The positive Z_{DR} column remained evident in association with the updraft. Within the three-body echo, Z_{DR} levels were distinctly positive at the trailing edge of the storm and sharply negative in the more distant portion of the appendage (Fig. 2f). These large Z_{DR} variations are partially due to the use of higher-elevation-angle PPI data for the interpolations at the grid points near the back edge of the storm versus the lower-elevation-angle data that were used to grid the more distant end of the three-body echo. Hubbert and Bringi (2000) have demonstrated that the Z_{DR} observed in three-body echoes is positive at higher-elevation angles and negative at lower-elevation angles. Additionally, Picca and Ryzhkov (2012) have shown that Z_{DR} tends to become negative toward the far-range end of long three-body echoes due to the larger contributing ground surface scattering area and the consequently smaller incidence angles. Organized areas of positive K_{DP} were not evident at the 6 km MSL analysis height; this was also true at greater analysis heights (not shown).

These two dual-Doppler analyses covered the critical time interval during which the decision to issue the severe thunderstorm warning was being made. The synthesized midlevel airflow fields confirmed the existence of an intensifying updraft within an anticyclonic flow

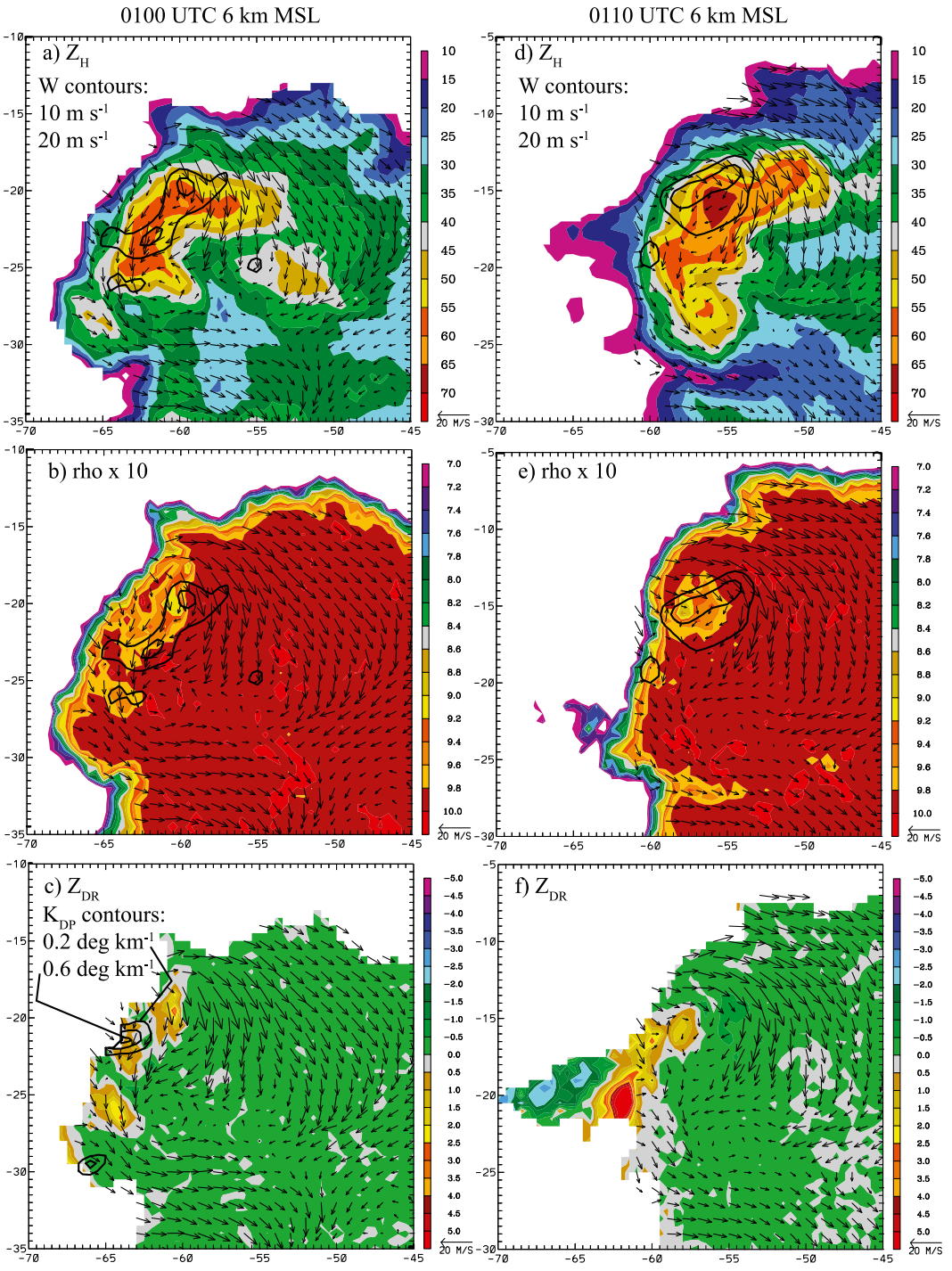

FIG. 2. Storm-relative dual-Doppler horizontal winds (m s^{-1}) in the developing Fort Collins hailstorm at 6 km MSL. Analysis times are (a)–(c) 0100 and (d)–(f) 0110 UTC. Underlying color-filled CSU-CHILL data fields are (a),(d) reflectivity (dBZ), (b),(e) $\rho_{HV} \times 10$, and (c),(f) Z_{DR} (dB). Grid origin is the CSU-CHILL radar.

pattern. In the high-reflectivity core associated with the updraft, the dual-polarization data implied that hail was likely growing aloft during this prewarning period. In particular, the local ρ_{HV} reductions to values of ~0.90–0.92 were probably due to the expanded variety of hydrometeor shapes and thermodynamic phases provided by graupel and hail particles whose growth was being supported by the updraft's moisture flux. The continually visible positive

Z_{DR} column confirmed that the updraft was capable of promoting appreciable concentrations of supercooled liquid water by lofting drops to subfreezing heights. The nonmeteorological characteristics of the dual-polarization data values in the three-body scattering echo helped call attention to the increasing development of this feature.

The storm structure and probable hail growth areas revealed by these dual-Doppler analyses have some mirror-image similarities to those reported during the Westplains, Colorado, hailstorm (Foote 1984). In that study, the millimeter-sized frozen ''embryos'' that subsequently grew into the largest diameter hailstones were advected into portions of the storm's primary updraft by midlevel storm-relative inflow that curved cyclonically along the southern side of the updraft [Figs. 1 and 3 in Foote (1984)]. In the July 2011 FCL hailstorm, the flanking midlevel inflow occurred along the northern side of the updraft due to the anticyclonically curved storm-relative airflow. The locally reduced–ρ_{HV} and enhanced positive–Z_{DR} values at the 6-km height observed in the northern portions of the main updraft were probably due to the rapid, potentially wet growth of the hail embryos as they entered the higher supercooled liquid water concentrations in the updraft, similar to the discussions of the graupel belt presented in Kumjian et al. (2010).

b. *Dual-polarization data fields in the 3.5°-elevation-angle PPI scans*

Because multiple-Doppler wind field syntheses are not routinely available in operational settings, the above analyses are designed to provide a general overview of the storm's primary organizational features as it intensified. In this section, the dual-polarization data fields are presented in the same PPI format that the warning forecaster would have available in real time.

The 3.5°-elevation-angle data were selected for this purpose because they intersected the storm's echo core at a height of ~5.2 km MSL (i.e., ~800 m below dual-Doppler analyses in Fig. 2). Based on the sounding data in Fig. 1, the environmental temperature at this height was ~−1°C, while the temperature of a surface-based parcel experiencing an undiluted moist-adiabatic ascent was ~+2°C. As emphasized in the NWS dual-polarization radar training materials, patterns observed in the polarimetric data fields can be of particular utility at height levels near the environmental freezing level. Selected data fields observed in each of the CSU-CHILL 3.5° PPI sweeps in the four volume scans conducted between 0059 and 0109 UTC are shown in Fig. 3. During the 0059 UTC volume scan, reflectivities exceeded 55 dBZ (Fig. 3a). A well-defined ρ_{HV} minimum, with values decreasing to ~0.90, was present within the dual-Doppler-indicated updraft (Fig. 3b). The positive Z_{DR} values associated with oblate hydrometeors in the updraft (see Fig. 2a) were evident along the leading edge of the core reflectivity gradient (Fig. 3c). Additional positive Z_{DR} areas were found near the down-range end of the echo core (i.e., generally west of $X = -63$ km) where the effects of three-body scattering would be expected to cause Z_{DR} artifacts.

Echo core reflectivities had intensified and expanded in area in the 0103 UTC volume scan, and the three-body scattering signature started to appear (Fig. 3d). The reduced-ρ_{HV} and positive-Z_{DR} column characteristics of the updraft remained evident (Figs. 3e,f). Both of these polarimetric variables continued to present distinctive values in the three-body scattering echo.

The 0106 UTC CSU-CHILL volume scan overlapped the KFTG 0104 UTC volume scan, during which forecaster attention was increasingly drawn to the storm. Pixels with reflectivity exceeding 65 dBZ became more numerous at the 3.5°-elevation angle (Fig. 4a), while regions of reduced ρ_{HV} (Fig. 4b) and positive Z_{DR} (Fig. 4c) persisted in the presumed region of hail growth in the updraft. The severe thunderstorm warning was issued as the 0109 UTC KFTG volume was being conducted. At this time, the 65-dBZ echo core became more consolidated (Fig. 4d). Much of the high-reflectivity core was also characterized by ρ_{HV} levels in the 0.90–0.94 range (Fig. 4e). The maximum reflectivity core became displaced farther eastward from the positive Z_{DR} column, with a small area of slightly negative Z_{DR} values beginning to appear immediately east of the core ($X = -54$, $Y = -14$ km; Fig. 4f). The combination of high Z_H, reduced ρ_{HV}, and Z_{DR} from zero to slightly negative is typical of precipitation volumes that contain significant concentrations of hail. These regions of reduced ρ_{HV} in the >50-dBZ echo core could be traced upward to heights of ~7.4 km MSL (ambient temperature of −18°C). Picca and Ryzhkov (2012) found that S-band ρ_{HV} levels were frequently less than 0.90 in the hail growth region from −10° to −20°C of a storm that produced 10-cm-diameter hail in Oklahoma. The ρ_{HV} reduction observed in the hail growth region of the FCL storm was probably less than that observed in the Oklahoma case due to the reduced Mie scattering effects associated with smaller hailstone diameters.

Melting can appreciably reduce the diameters of hailstones as they descend toward the surface. Thus, in addition to the above-described examinations of dual-polarization data near the freezing level, low-elevation-angle data should also be examined during the warning decision process. Figure 5a shows several data fields in the 0.5°-elevation sweep as the CSU-CHILL volume scan began at 0109 UTC. As per the WDTB training materials, the simultaneous occurrence of ~0-dB Z_{DR} values and ρ_{HV} magnitudes well below 0.95 within the high-reflectivity

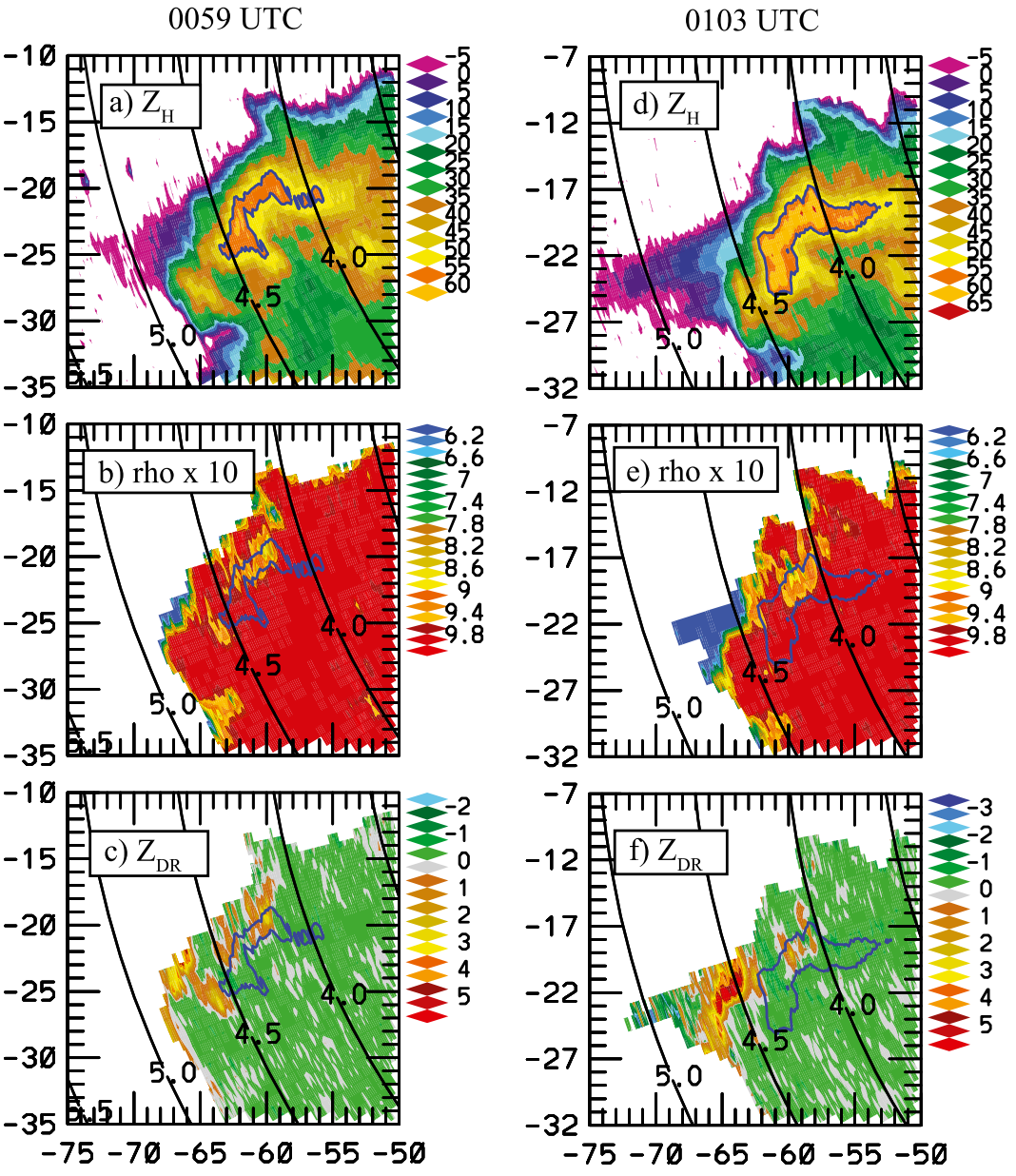

FIG. 3. CSU-CHILL 3.5°-elevation-angle PPI scan data at (a)–(c) 0059 and (d)–(f) 0103 UTC 14 Jul 2011. Color-filled fields are (top) reflectivity (dBZ), (middle) $\rho_{HV} \times 10$, and (bottom) Z_{DR} (dB). Solid blue line is the 55-dBZ reflectivity contour. Concentric arcs are AGL heights (km) on the PPI scan surface. (Add 1.42 km to convert to MSL heights.) Grid origin is the CSU-CHILL radar. Note that color scales differ from those used in the constant altitude PPI (CAPPI) plots shown in Fig. 2.

(>55 dBZ) echo core provided strong confirmation that the hailstones were surviving to near-surface heights (i.e., they were large enough to resist significant melting effects.) The K_{DP} values of ~3° km^{-1} indicated that heavy rain was also present in several localized regions of the echo core. Indications of melting hail were much more evident in a low-elevation scan taken near the end of the observed hail swath at 0158 UTC (Fig. 5b). The echo core Z_{DR} levels had become positive, and both ρ_{HV} and K_{DP} had increased significantly in comparison to the 0109 UTC observations. Based on data collected by Community Collaborative Rain, Hail, and Snow Network (CoCoRaHS) volunteer observers, hail diameters had decreased to 8–15 mm (0.3–0.6 in.) after 0150 UTC. The force balance acting on the water coating of melting hailstones in this diameter range typically causes the meltwater to accumulate around the equatorial region of the drop, yielding an oblate cross section (Rasmussen et al. 1984). Hailstones that

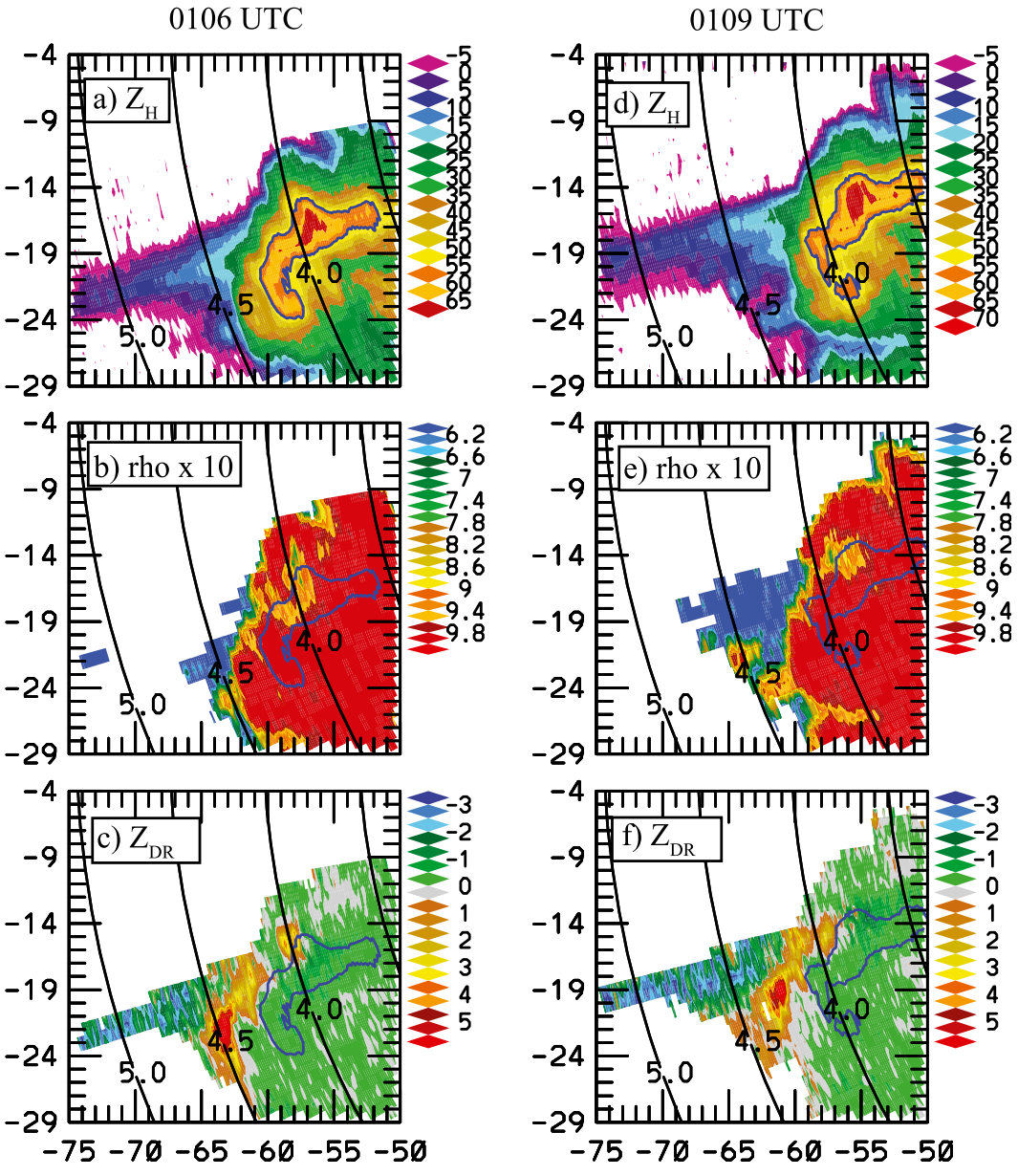

FIG. 4. As in Fig. 3, but for (left) 0106 and (right) 0109 UTC.

completely melt form large (~8 mm)-diameter raindrops whose equilibrium shapes are distinctly flattened. The production of these small, water-stabilized, frozen hydrometeors and large liquid drops in areas of hail melting tends to shift the dual-polarization signatures toward the values associated with rain (positive Z_{DR} and K_{DP}; high ρ_{HV}).

Based on the trends in the WSR-88D data, the warning forecaster began to more carefully scrutinize the storm's radar presentation during the KFTG volume scan that started at 0104 UTC. Postanalysis of the CSU-CHILL dual-polarization data provided additional evidence of the storm's hail production during the time period when the warning issuance decision was being developed. At 0059 UTC, the presence of a vigorous updraft was indicated by the positive Z_{DR} values associated with the oblate raindrops that were being lofted/size sorted near the environmental temperature level from ~−3° to −5°C. Within the expanding and intensifying >55-dBZ echo core region, ρ_{HV} levels decreased toward the 0.90 range, suggesting that growing hailstones were contributing to an increasingly broad distribution of hydrometeor shapes and orientations. Distinctive Z_{DR} and ρ_{HV} patterns also helped highlight the developing three-body scattering echo that became

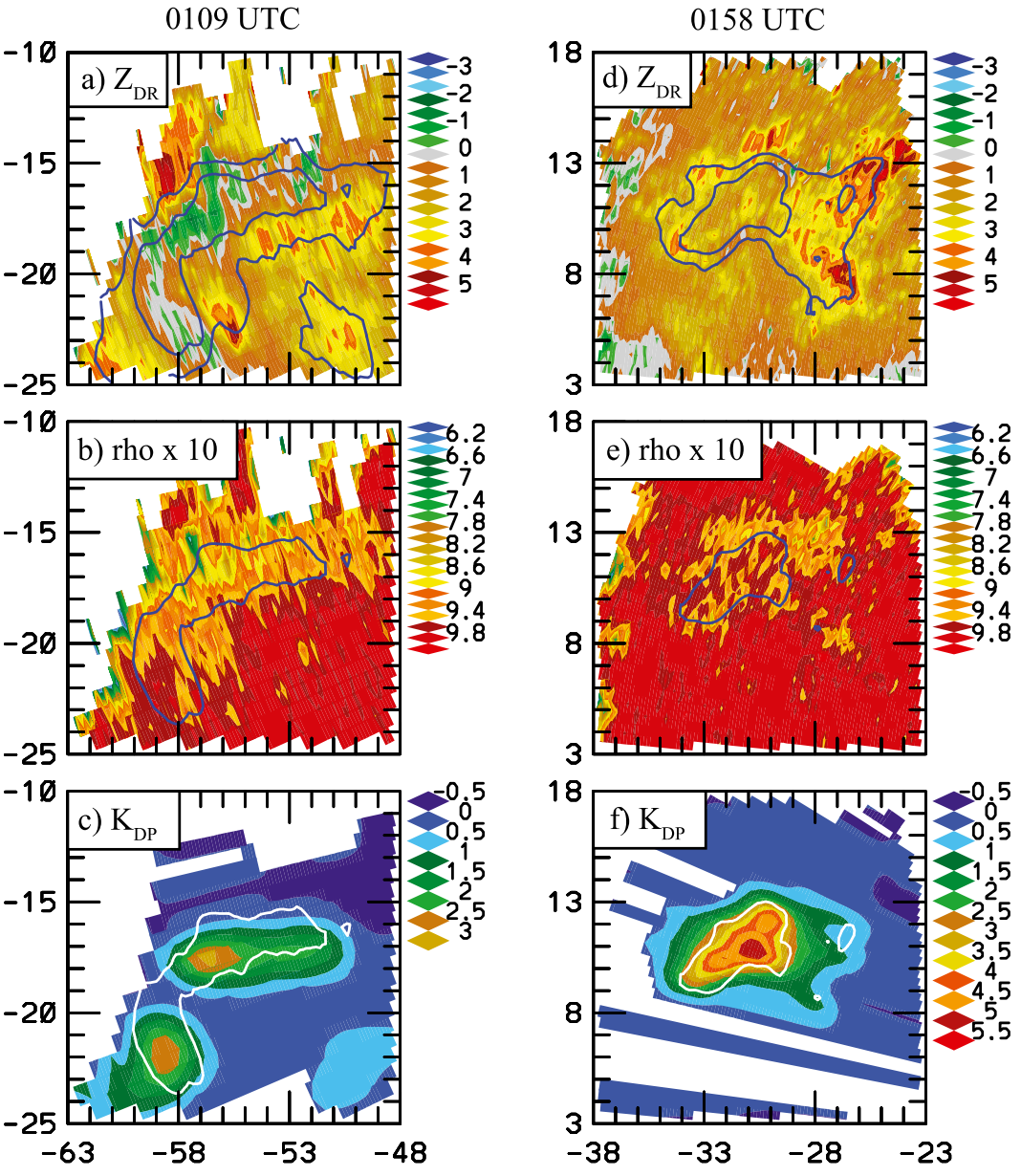

FIG. 5. CSU-CHILL low-elevation-angle PPI scan data at (a)–(c) warning issuance time (0109 UTC) and (d)–(f) the end of the hail swath/subsevere-hail-diameter time (0158 UTC). Elevation angles are 0.5° and 1.0° at 0109 and 0158 UTC, respectively. Color-filled data fields are (top) Z_{DR} (dB), (middle) $\rho_{HV} \times 10$, and (bottom) K_{DP} (° km^{-1}). Solid contour lines are 45 and 55 dBZ in the (top) and 55 dBZ only in the (middle),(bottom). Horizontal axes are distances (km) from CSU-CHILL.

prominent down range of the high-reflectivity/reduced-ρ_{HV} echo core observed in the 3.5° PPI CSU-CHILL data. The presence of near-0-dB Z_{DR} and $\rho_{HV} < 0.95$ in the high-reflectivity-echo core at the 0.5°- elevation angle confirmed that larger hailstones, with limited evidence of melting, were mixing with the near-surface precipitation at 0109 UTC. The dual-polarization indications that hail was actively growing aloft and was eventually reaching the surface are useful for improving both the confidence level, and possibly the lead time, with which severe thunderstorm warnings are issued.

4. Variations in cloud-to-ground lightning polarity characteristics among the 14 July 2011 storms in the WFO Denver/Boulder County warning area

In addition to the microphysical insights provided by dual-polarization radar data, the characteristics of

cloud-to-ground lightning activity can be useful in evaluating thunderstorms. Operational mapping of lightning within the United States is provided by NLDN (Rudlosky and Fuelberg 2010). The NLDN equipment processes the first few microseconds of the waveforms received from lightning radiation at very low frequencies [~10 kHz; Krider et al. (1976)]. This leading segment of the signal emanates from the initial portion of the high current return stroke of cloud-to-ground discharges. It provides both an accurate position reference for the ground contact point and information on the magnitude and direction of the current flow (flash polarity). By combining the lines of position obtained from multiple stations, the NLDN obtains a median discharge location accuracy of ~0.5 km (Cummins and Murphy 2009). The lightning locations and current polarities obtained from the NLDN network can be overlaid with the real-time WSR-88D data displayed by the Advanced Weather Interactive Processing System (AWIPS).

Within thunderstorm updrafts, noninductive electrification occurs due to the rebounding collisions between ice crystals and graupel particles in the temperature range from ~−10° to −25°C (Williams et al. 1991; MacGorman et al. 2008). Charging is most significant when these collisions take place in the presence of supercooled water. For a large range of thermodynamic states, the graupel particles charge negatively and the ice crystals charge positively following these collisions. The subsequent differential vertical motions experienced by the particles produce two of the primary charge centers observed in thunderstorms with positive charge residing aloft near −40°C and negative charge at lower heights near ~−20°C (Stolzenburg et al. 1998). When the riming rate is sufficiently enhanced due to high supercooled liquid water contents (i.e., conditions conducive for the wet growth of hailstones), the charging sense can reverse, producing positive charge at midlevels (Saunders 1993). This reduced-height positive charge center can be the source of the "positive CG" discharges that lower positive charge to ground (MacGorman et al. 2005; Wiens et al. 2005). Associations have been found between thunderstorms that generate high percentages of positive polarity cloud-to-ground discharges and severe weather activity (Reap and MacGorman 1989; Stolzenburg 1994). In a more detailed examination of this association, Lang and Rutledge (2002) found that storms that produced predominately positive CG lightning were characterized by relatively large volumes of strong updrafts (>10–20 m s^{-1}). To a first approximation, the high supercooled liquid water concentrations that promote positive charging on the rimer and increased positive CG lightning also favor the growth of hailstones. Thus, while the severe thunderstorm activity can occur in the absence of significant positive CG production (MacGorman and Burgess 1994), monitoring the trends in the NLDN lightning polarity can help identify storms that may pose a hail threat.

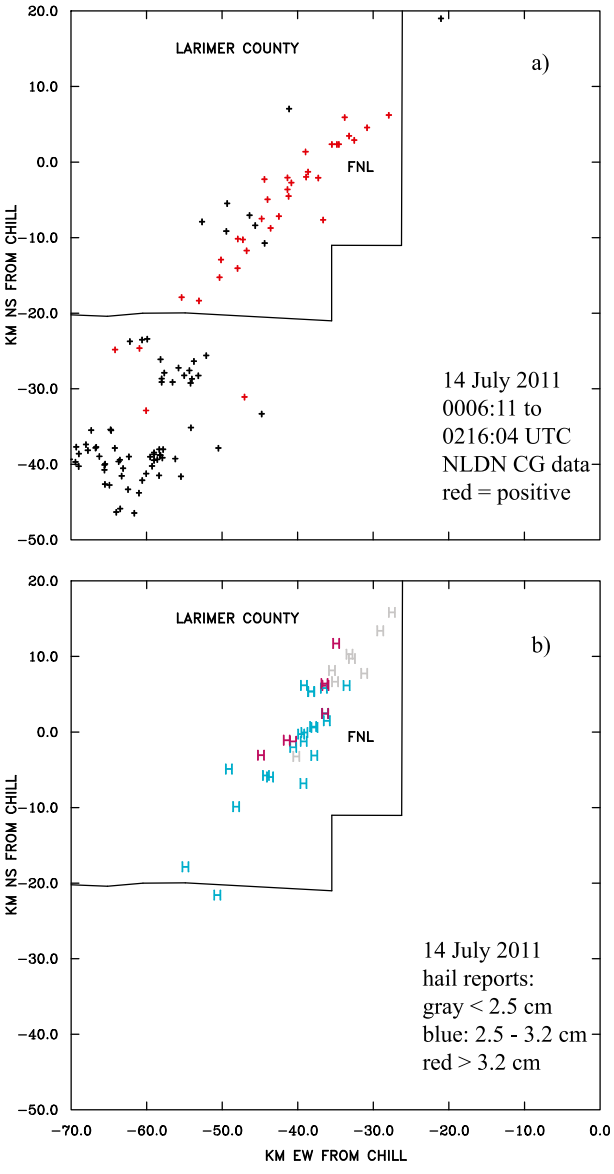

FIG. 6. (a) Locations of NLDN CG discharges along the path of the Fort Collins hailstorm across Larimer County. Black symbols designate negative polarity flashes, while positive polarity discharges are shown in red. (b) Locations of hail reports from the Fort Collins hailstorm. Geographic reference point FNL is the Fort Collins–Loveland Municipal Airport.

The geographical distribution of NLDN CG lightning polarity and surface hail reports for the FCL hailstorm is shown in Fig. 6. Positive CG discharges with currents less than +15 kilo Ampère (kA) were disregarded to avoid contamination from in-cloud activity (Rudlosky and Fuelberg 2010). A small number of data points that had elliptical location uncertainty errors larger than

10 km were also removed. The lightning polarity was primarily negative as the storm was developing south of Larimer County (Fig. 6a). The shift toward increasing positive polarity CG activity began around 0106 UTC. Based upon spotter reports, observations of hail diameters of 25 mm (1 in.) or larger started at ~0110 UTC. The close association between the locations of the hail reports and the positive CG flashes continued through most of the storm's lifetime (Fig. 6b).

Strong correlations have been found between lightning activity and the volume of graupel located within updrafts in the temperature range from ~−5° to −30°C (Wiens et al. 2005; Deierling et al. 2008). Increases in updraft speed, and particularly updraft width, promote more frequent lightning (Lang and Rutledge 2002) and enhance hail production (Nelson 1983). To explore this relationship for this case, time–height plots were prepared from the CSU-CHILL gridded data. For these purposes, L_{DR} was used as the primary dual-polarization variable associated with graupel and hail. Variable L_{DR} is based on the ratio of the strength of the linear scale cross-polarized received signal relative to that of the conventional copolarized received signal:

$$L_{DR} = 10\,\mathrm{Log}_{10}(Z_{vh}/Z_{hh}), \tag{3}$$

where the received and transmitted polarizations are given by the first and second subscripts next to Z, respectively. [The simultaneous transmission of essentially identical H- and V-polarized waves by the upgraded WSR-88D radars prevents the reception of the cross-polar "off channel" term in the numerator of the argument of the logarithm in Eq. (3); L_{DR} is not available from the upgraded WSR-88D radars.] The cross-polar return signal is increased by the presence of nonspherical hydrometeors with major axes that are not aligned with the H- and V-polarization planes. The cross-polar signal is further enhanced when the dielectric properties of the hydrometeors approach those of water versus ice. Thus, irregularly shaped graupel and hail particles, especially when their outer surfaces are wet (owing to wet growth), and freezing drops, will increase L_{DR}. In the time–height plots shown in Fig. 7, grid points where L_{DR} was greater than −25 dB and reflectivity was greater than 40 dBZ at heights between 5.5 and 8 km MSL were assumed to indicate the presence of graupel. These values correspond to the levels where the graupel hydrometeor category membership functions for reflectivity and L_{DR} in the hydrometeor classification system presented in Tessendorf et al. (2005) reach 0.5. It should be recognized that variations in graupel density, shape, orientation angle distributions, etc. necessarily produce uncertainties in these "graupel threshold" values. Based on the 0.5-km

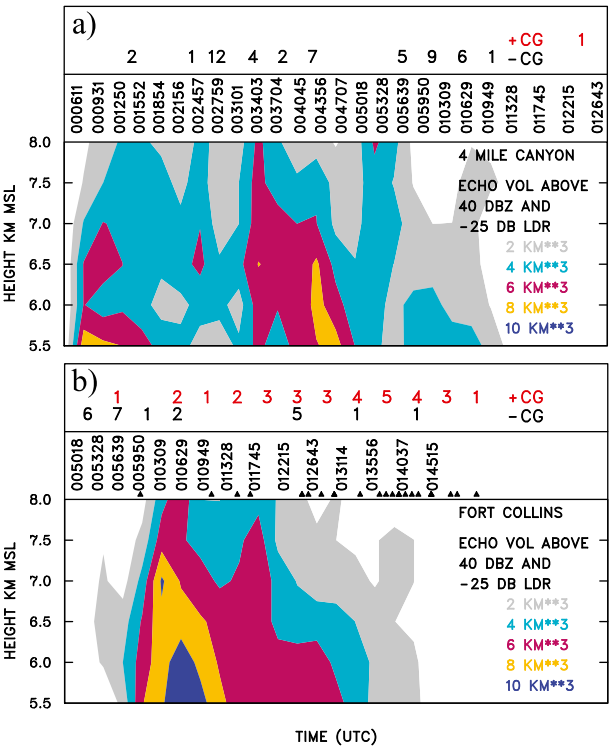

FIG. 7. Time–height plots of CSU-CHILL data. Color-fill pattern depicts Cartesian analysis grid volumes where reflectivity is greater than or equal to 40 dBZ and L_{DR} is greater than or equal to −25 dB. Volume scan starting times are shown with vertically oriented numbers. Triangles show the times of spotter reports of large (2.5 cm or greater)-diameter hail. NLDN positive and negative discharge counts during each KFTG volume scan are listed across the top of the plot. Data from the (a) flash-flood-producing Fourmile Canyon storm and (b) Fort Collins hailstorm.

3D gridpoint spacings, the graupel gridpoint counts were converted to volumetric values at each analysis height and time. To provide a comparative reference, Fig. 7a shows the history for the storm that produced flash flooding in the Fourmile canyon (event two in the storm sequence described in the introduction). While this storm generated heavy rainfall, it produced no reports of 2.5 cm or larger hail in the Storm Prediction Center records. This storm affected a less populated foothills area, lessening the probability of obtaining spotter reports. Also, observations made by local residents and precipitation disdrometers operated by NCAR both indicated that some hail occurred in the Fourmile Canyon storm (Matrosov et al. 2013). The graupel volume in the Fourmile Canyon storm was briefly maximized during the CSU-CHILL volume scans at 0043:56 and 0047:07 UTC. While the NLDN CG counts reached a localized maximum of seven per radar volume scan a few minutes earlier during the 0040:45 UTC volume, all of the flashes were of negative polarity. Only a single positive CG discharge near the Fourmile Canyon

storm occurred much later during the 0122:15 UTC volume, as the storm was dissipating.

The time–height history of the FCL storm showed that graupel existed throughout a larger volume and extended through a greater height range in comparison to the Fourmile Canyon storm (Fig. 7b; 0103:09–0113:28 UTC volumes). During this same general time period, the CG polarity began a long-term switch to positive polarity at 0109:49 UTC—very close to the time of the initial severe thunderstorm warning issuance and the beginning of the damaging hail swath. As suggested by the results of Wiens et al. (2005), the larger graupel volume detected in the FCL was likely indicative of a more extensive area of strong updrafts with large supercooled liquid water concentrations that would have promoted both the generation of a lower positive charge center (favoring + CG flashes) and vigorous hail growth. The continuing production of + CG flashes and spotter reports of large hail seen in Fig. 7b after ~0120 UTC is likely related to the general descent of the reflectivity centroid following the initial period of rapid updraft intensification, bringing positively charged, large ice hydrometeors closer to the surface (Carey et al. 2003).

In addition to the FCL storm, damaging hail was generated by a storm that affected Denver International Airport (KDEN) later in the evening of 13 July 2011 (event four in the introduction). The CSU-CHILL radar was conducting low-elevation rain-mapping scans during this event, so graupel volume estimations like those shown in Fig. 7 could not be prepared. Also, because KDEN is only ~10 km from the KFTG radar site, the maximum elevation angle scanned by this radar was too low to observe much of the mid- and upper-level structure of the hailstorm that struck the airport. Instead, observations made by the Cheyenne, Wyoming, WSR-88D (KCYS; 352° at 153 km from KFTG) were used to characterize the KDEN hailstorm. Reflectivity data from KCYS were interpolated onto a 3D Cartesian grid with a mesh size of 1.0 km in the X, Y, and Z directions. To ensure coverage to echo top, the maximum analysis height was 14 km MSL. Within the horizontal domain, the data-processing limits were adjusted to follow the storm motion and to exclude echoes associated with neighboring storms. Counts of the number of grid points where reflectivity exceeded 40 and 50 dBZ were developed for all analysis heights between 5.5 and 14 km MSL; these gridpoint summations were then converted to atmospheric volumes. The resultant time history plot of the KCYS data from the KDEN storm is shown in Fig. 8a. The volume values are greater than those seen in Fig. 7 because heights above 8.5 km MSL are included and no L_{DR} data were available to allow the application of an additional graupel detection threshold. Hailstones with

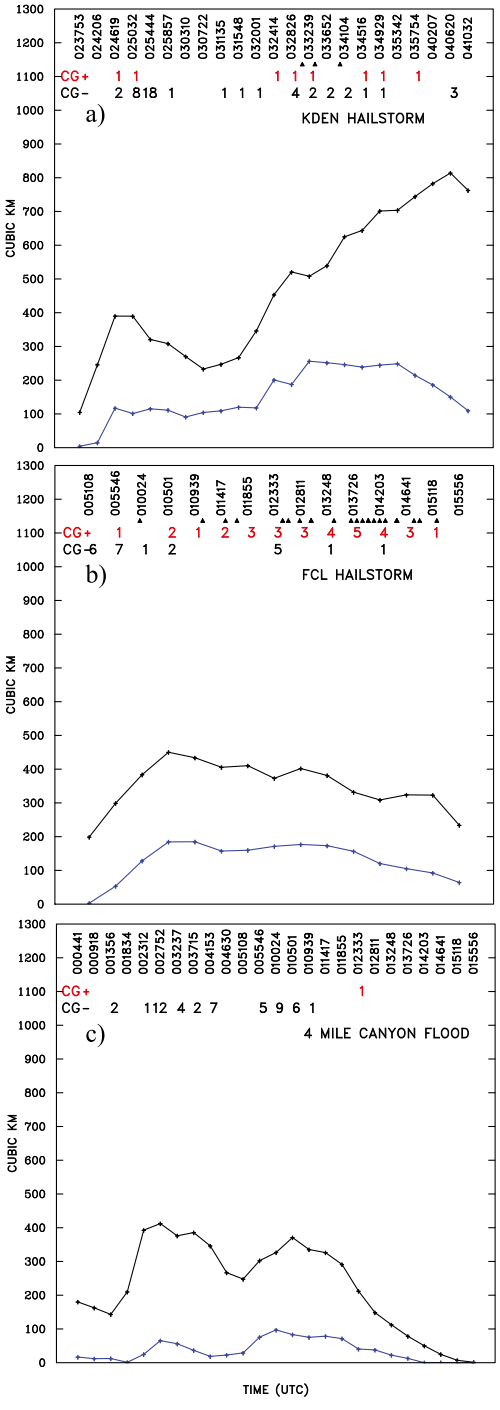

FIG. 8. Time history plots of selected reflectivity volume values from WSR-88D observations. Black trace is the volume with reflectivities at or above 40 dBZ. Blue trace is volume with reflectivities at or above 50 dBZ: (a) the Denver International Airport hailstorm, (b) the Fort Collins storm, and (c) the Fourmile Canyon storm. Counts of the positive and negative NLDN-detected CG flashes during each volume scan are listed immediately below the WSR-88D volume scan start times. Triangles mark the times when spotter reports of large (2.5-cm diameter or greater) hail were received.

diameters of 2.5 cm, driven by surface wind squalls of 26 m s^{-1}, began to affect the airport at 0331 UTC. This was ~10–15 min after the 40- and 50-dBZ echo volumes began to markedly increase with time. Positive CG activity began to occur during the volume scan that started at 0324:14 UTC just as the storm reached the southern boundary of the airport, but the majority of the flashes were of negative polarity. Also, a brief earlier episode of positive CG activity was associated with a period of rapid echo volume growth around 0242 UTC.

For comparison, similar time history plots were prepared from the KFTG data collected from the FCL hailstorm and the Fourmile Canyon flash flooding storm. As in the KDEN case, the onset of positive CG activity in the FCL storm began ~10 min after the 40- and 50-dBZ echo volumes in the 5.5–14 km MSL height range began to increase around 0055 UTC (Fig. 8b). The 40-dBZ echo volume in the Fourmile Canyon storm reached peak values that were comparable to those observed in the FCL hailstorm (Fig. 8c). However, the 50-dBZ echo volume in the Fourmile Canyon storm was only ~50% of that observed in the FCL storm. This smaller 50-dBZ echo volume in the Fourmile Canyon storm suggests that it contained some combination of weaker and/or less spatially extensive updrafts than did the FCL or KDEN storms. In contrast to the FCL and KDEN storms, the Fourmile Canyon storm produced relatively little positive CG lightning activity and no reports of severe hail.

5. Summary

The single-polarization data provided by the KFTG radar properly drew the warning forecaster's attention to the developing Fort Collins storm. During this prewarning period, the KFTG radial velocity pattern displayed increasing evidence of local wind speed accelerations around the midlevel flanks of the storm, indicating that an updraft with a magnitude and size sufficient to maintain a core that experienced minimal environmental mixing existed (Miller et al. 1990). Both the intensifying reflectivity fields present on the individual PPI sweeps and the VIL calculations generated by KFTG radar product generator confirmed that the storm was rapidly strengthening. An increasingly prominent three-body scattering signature provided further evidence of a growing mass of hydrometeors aloft and, thus, a greater potential to generate severe hail at the surface.

The CSU-CHILL dual-polarization data provided additional information to infer the presence of hail at heights near the freezing level in the developing storm. The positive Z_{DR} column helped to more specifically identify the location of an updraft whose strength and size was sufficient to loft oblate raindrops above the freezing level and to promote the size sorting of these drops. The resultant reduction in the population of small (<2-mm diameter), more spherical drops was probably one important factor in making the Z_{DR} values more positive in the updraft (Brandes et al. 1995). A region containing ρ_{HV} values between 0.92 and 0.94 generally encompassed portions of both the positive Z_{DR} column and the reflectivity core in the PPI data near the environmental temperature level from −2° to −5 °C. This reduced-ρ_{HV} region showed good spatial correlation with the stronger updrafts identified by dual-Doppler analyses. The ρ_{HV} values in this area were probably being reduced due to growing hailstones that increased the diversity of hydrometeor shapes and orientations (Balakrishnan and Zrnić 1990). The increasing numbers and diameters of these hailstones contributed to the development of reflectivity levels in excess of 60 dBZ in the reduced-ρ_{HV} region. Melting effects will reduce the diameters of hailstones as they descend into above-freezing temperatures, with smaller-diameter hailstones completely melting into raindrops prior to reaching the surface. Thus, even when clear dual-polarization indications of hail development aloft are observed, distinct shifts toward positive Z_{DR} and K_{DP} values with increasing distance below the melting level in the echo core indicate that appreciable hail melting and drop shedding are occurring (Ryzhkov et al. 2013). In addition to dual-polarization radar data, warning issuance decisions will continue to involve forecaster evaluation of the structural reflectivity characteristics of thunderstorms, their knowledge of the mesoscale meteorological environment, the contents of spotter reports, etc.

The polarity characteristics of the NLDN-detected CG flashes provided an additional indication of updraft vigor and the related hail production capabilities of several of the individual storms that were observed on 14 July 2012. The FCL hailstorm displayed a distinct shift to predominantly positive polarity cloud-to-ground flashes as the initial severe thunderstorm warning was being issued. The production of positive CG discharges continued through the time period during which reports of hail diameters of ~2.5 cm were being received. Different lightning polarity characteristics were noted in the two other storms of 14 July 2011 that were analyzed. The storm that caused damaging hail at Denver International Airport produced only a small increase in positive discharges relative to a larger number of negative flashes as it entered its hail-generation stage. The Fourmile Canyon storm produced essentially no positive CG lightning and also no severe hail reports. It appears that the monitoring of positive CG lightning trends can help identify storms with relatively strong, horizontally extensive updrafts (Lang and Rutledge 2002;

Bruning et al. 2012). These updraft characteristics provide the copious amounts of supercooled water that promote both the development of positively charged rimers and the efficient production of hail via the wet growth process. However, it must also be recognized that storms that generate little or no positive CG lightning can also produce severe weather (MacGorman and Burgess 1994).

Thunderstorm developments in the WFO Denver/Boulder County warning area between 0000 and 0400 UTC 14 July 2011 posed several challenges to operational forecasters. Warning issuances were required for multiple storms that separately produced flash flooding and damaging hail. None of these storms displayed clear radar evidence of the supercellular organization that is well known to warning forecasters. The results of this study indicate that careful examination of dual-polarization radar data from near the environmental freezing level, along with the CG lightning mapping capabilities of the NLDN system, can help diagnose the severe weather threat posed by shorter-lived, pulse-type storms.

Acknowledgments. Comments provided by Paul Schlatter (NOAA) and two anonymous reviewers materially improved the original version of this paper. Support for the first two authors and for the CSU-CHILL national radar facility is provided by the National Science Foundation through Cooperative Agreement AGS1138116.

REFERENCES

Amburn, S. A., and P. L. Wolf, 1997: VIL density as a hail indicator. *Wea. Forecasting,* **12,** 473–478, doi:10.1175/1520-0434(1997)012<0473:VDAAHI>2.0.CO;2.

Aydin, K., T. A. Seliga, and V. Balaji, 1986: Remote sensing of hail with a dual linear polarization radar. *J. Climate Appl. Meteor.,* **25,** 1475–1484, doi:10.1175/1520-0450(1986)025<1475:RSOHWA>2.0.CO;2.

Balakrishnan, N., and D. S. Zrnić, 1990: Use of polarization to characterize precipitation and discriminate large hail. *J. Atmos. Sci.,* **47,** 1525–1540, doi:10.1175/1520-0469(1990)047<1525:UOPTCP>2.0.CO;2.

Brandes, E. A., J. Vivekanandan, J. D. Tuttle, and C. J. Kessenger, 1995: A study of thunderstorm microphysics with multiparameter radar and aircraft observations. *Mon. Wea. Rev.,* **123,** 3129–3143, doi:10.1175/1520-0493(1995)123<3129:ASOTMW>2.0.CO;2.

Bruning, E. C., S. A. Weiss, and K. M. Calhoun, 2012: Continuous variability in thunderstorm primary electrification and an evaluation of inverted-polarity terminology. *Atmos. Res.,* **135–136,** 274–284, doi:10.1016/j.atmosres.2012.10.009.

Carey, L. D., W. A. Petersen, and S. A. Rutledge, 2003: Evolution of cloud-to-ground lightning and storm structure in the Spencer, South Dakota, tornadic supercell of 30 May 1998. *Mon. Wea. Rev.,* **131,** 1811–1831, doi:10.1175//2566.1.

Cummins, K. L., and M. J. Murphy, 2009: An overview of lightning locating systems: History, techniques, and data uses, with an in-depth look at the U.S. NLDN. *IEEE Trans. Electromagn. Compat.,* **51,** 499–518, doi:10.1109/TEMC.2009.2023450.

Deierling, W., W. A. Petersen, J. Latham, S. Ellis, and H. J. Christian, 2008: The relationships between lightning activity and ice fluxes in thunderstorms. *J. Geophys. Res.*, **113,** D15201, doi:1029/2007JD009700.

Foote, G. B., 1984: A study of hail growth using observed storm conditions. *J. Climate Appl. Meteor.,* **23,** 84–101, doi:10.1175/1520-0450(1984)023<0084:ASOHGU>2.0.CO;2.

Herzegh, P. H., and A. R. Jameson, 1992: Observing precipitation through dual-polarization radar measurements. *Bull. Amer. Meteor. Soc.,* **73,** 1365–1374, doi:10.1175/1520-0477(1992)073<1365:OPTDPR>2.0.CO;2.

Higgins, R. W., Y. Yao, and X. L. Wang, 1997: Influence of the North American monsoon system on the U.S. summer precipitation regime. *J. Climate,* **10,** 2600–2622, doi:10.1175/1520-0442(1997)010<2600:IOTNAM>2.0.CO;2.

Hubbert, J. C., and V. N. Bringi, 2000: The effects of three-body scattering on differential reflectivity signatures. *J. Atmos. Oceanic Technol.,* **17,** 51–61, doi:10.1175/1520-0426(2000)017<0051:TEOTBS>2.0.CO;2.

Jameson, A. R., 1985: Microphysical interpretation of multiparameter radar measurements in rain. Part III: Interpretation and measurement of propagation differential phase shift between orthogonal linear polarizations. *J. Atmos. Sci.,* **42,** 607–614, doi:10.1175/1520-0469(1985)042<0607:MIOMRM>2.0.CO;2.

Knight, C. A., and N. C. Knight, 1970: The falling behavior of hailstones. *J. Atmos. Sci.,* **27,** 667–671, doi:10.1175/1520-0469(1970)027<0667:LSOH>2.0.CO;2.

Krider, E. P., R. C. Noggle, and M. Uman, 1976: A gated, wideband magnetic direction finder for lightning return strokes. *J. Appl. Meteor.,* **15,** 301–306, doi:10.1175/1520-0450(1976)015<0301:AGWMDF>2.0.CO;2.

Kumjian, M. R., and A. V. Ryzhkov, 2008: Polarimetric signatures in supercell thunderstorms. *J. Appl. Meteor. Climatol.,* **47,** 1940–1961, doi:10.1175/2007JAMC1874.1.

——, and ——, 2012: The impact of size sorting on the polarimetric radar variables. *J. Atmos. Sci.,* **69,** 2042–2060, doi:10.1175/JAS-D-11-0125.1.

——, ——, V. M. Melinkov, and T. J. Schuur, 2010: Rapid-scan, super-resolution observations of a cyclic supercell with a dual-polarization WSR-88D. *Mon. Wea. Rev.,* **138,** 3762–3768, doi:10.1175/2010MWR3322.1.

Lang, T. J., and S. A. Rutledge, 2002: Relationships between convective storm kinematics, precipitation, and lightning. *Mon. Wea. Rev.,* **130,** 2492–2506, doi:10.1175/1520-0493(2002)130<2492:RBCSKP>2.0.CO;2.

Lemon, L. R., 1998: The radar "three body scattering spike": An operational large hail signature. *Wea. Forecasting,* **13,** 327–340, doi:10.1175/1520-0434(1998)013<0327:TRTBSS>2.0.CO;2.

Loney, M. L., D. S. Zrnić, J. M. Straka, and A. V. Ryzhkov, 2002: Enhanced polarimetric signatures above the melting level in a supercell thunderstorm. *J. Appl. Meteor.,* **41,** 1179–1194, doi:10.1175/1520-0450(2002)041<1179:EPRSAT>2.0.CO;2.

MacGorman, D. R., and D. W. Burgess, 1994: Positive cloud-to-ground lightning in tornadic storms and hailstorms. *Mon. Wea. Rev.,* **122,** 1671–1697, doi:10.1175/1520-0493(1994)122<1671:PCTGLI>2.0.CO;2.

——, W. D. Rust, P. Krehbiel, W. Rison, and E. Bruning, 2005: The electrical structure of two supercell storms during STEPS. *Mon. Wea. Rev.,* **133,** 2583–2607, doi:10.1175/MWR2994.1.

——, and Coauthors, 2008: TELEX: The Thunderstorm Electrification and Lightning Experiment. *Bull. Amer. Meteor. Soc.,* **89,** 997–1010, doi:10.1175/2007BAMS2352.1.

Matrosov, S. Y., R. Cifelli, and D. Gochis, 2013: Measurements of heavy convective rainfall in the presence of hail in flood-prone areas using an X-band polarimetric radar. *J. Appl. Meteor. Climatol.,* **52,** 395–407, doi:10.1175/JAMC-D-12-052.1.

Miller, L. J., J. D. Tuttle, and G. B. Foote, 1990: Precipitation production in a large Montana hailstorm: Airflow and particle growth trajectories. *J. Atmos. Sci.,* **47,** 1619–1646, doi:10.1175/1520-0469(1990)047<1619:PPIALM>2.0.CO;2.

Mohr, C. G., and R. L. Vaughn, 1979: An economical procedure for Cartesian interpolation and display of reflectivity factor in three dimensional space. *J. Appl. Meteor.,* **18,** 661–670, doi:10.1175/1520-0450(1979)018<0661:AEPFCI>2.0.CO;2.

——, L. J. Miller, R. L. Vaughan, and H. W. Frank, 1986: On the merger of mesoscale data sets into a common Cartesian format for efficient and systematic analysis. *J. Atmos. Oceanic Technol.,* **3,** 143–161, doi:10.1175/1520-0426(1986)003<0143:TMOMDI>2.0.CO;2.

Nelson, S. P., 1983: The influence of storm flow structure on hail growth. *J. Atmos. Sci.,* **40,** 1965–1983, doi:10.1175/1520-0469(1983)040<1965:TIOSFS>2.0.CO;2.

Picca, J., and A. Ryzhkov, 2012: A dual-wavelength polarimetric analysis of the 16 May 2010 Oklahoma City extreme hailstorm. *Mon. Wea. Rev.,* **140,** 1385–1403, doi:10.1175/MWR-D-11-00112.1.

Rasmussen, E. N., and D. O. Blanchard, 1998: A baseline climatology of sounding-derived supercell and tornado forecast parameters. *Wea. Forecasting,* **13,** 1148–1164, doi:10.1175/1520-0434(1998)013<1148:ABCOSD>2.0.CO;2.

Rasmussen, R. M., and A. J. Heymsfield, 1987: Melting and shedding of graupel and hail. Part I: Model physics. *J. Atmos. Sci.,* **44,** 2754–2763, doi:10.1175/1520-0469(1987)044<2754:MASOGA>2.0.CO;2.

——, V. Levizzani, and H. R. Pruppacher, 1984: A wind tunnel and theoretical study on the melting behavior of atmospheric ice particles: III. Experiment and theory for spherical ice particles of radius >500 μm. *J. Atmos. Sci.,* **41,** 381–388, doi:10.1175/1520-0469(1984)041<0381:AWTATS>2.0.CO;2.

Reap, R. M., and D. R. MacGorman, 1989: Cloud-to-ground lightning: Climatological characteristics and relationships to model fields, radar observations, and severe local storms. *Mon. Wea. Rev.,* **117,** 518–535, doi:10.1175/1520-0493(1989)117<0518:CTGLCC>2.0.CO;2.

Rotunno, R., and J. B. Klemp, 1982: The influence of the shear-induced pressure gradient on thunderstorm motion. *Mon. Wea. Rev.,* **110,** 136–151, doi:10.1175/1520-0493(1982)110<0136:TIOTSI>2.0.CO;2.

Rudlosky, S. D., and H. E. Fuelberg, 2010: Pre- and postupgrade distributions of NLDN reported cloud-to-ground lightning characteristics in the contiguous United States. *Mon. Wea. Rev.,* **138,** 3623–3633, doi:10.1175/2010MWR3283.1.

Ryzhkov, A., M. Kumjian, S. Ganson, and A. Khain, 2013: Polarimetric radar characteristics of melting hail. Part I: Theoretical simulations using spectral microphysical modeling. *J. Appl. Meteor. Climatol.,* **52,** 2849–2870, doi:10.1175/JAMC-D-13-073.1.

Saunders, C. P. R., 1993: A review of thunderstorm electrification processes. *J. Appl. Meteor.,* **32,** 642–655, doi:10.1175/1520-0450(1993)032<0642:AROTEP>2.0.CO;2.

Stolzenburg, M., 1994: Observations of high ground flash densities of positive lightning in summertime thunderstorms. *Mon. Wea. Rev.,* **122,** 1740–1750, doi:10.1175/1520-0493(1994)122<1740:OOHGFD>2.0.CO;2.

——, W. D. Rust, and T. C. Marshall, 1998: Electrical structure in thunderstorm convective regions: 3. Synthesis. *J. Geophys. Res.,* **103,** 14 097–14 108, doi:10.1029/97JD03545.

Tessendorf, S. A., L. J. Miller, K. C. Weins, and S. A. Rutledge, 2005: The 29 June 2000 supercell observed during STEPS. Part I: Kinematics and microphysics. *J. Atmos. Sci.,* **62,** 4127–4150, doi:10.1175/JAS3585.1.

Wiens, K. C., S. A. Rutledge, and S. A. Tessendorf, 2005: The 29 June 2000 supercell observed during STEPS. Part II: Lightning and charge structure. *J. Atmos. Sci.,* **62,** 4151–4177, doi:10.1175/JAS3615.1.

Williams, E. R., R. Zhang, and J. Rydcok, 1991: Mixed-phase microphysics and cloud electrification. *J. Atmos. Sci.,* **48,** 2195–2203, doi:10.1175/1520-0469(1991)048<2195:MPMACE>2.0.CO;2.

Wilson, J. W., and D. Reum, 1988: The flare echo: Reflectivity and velocity signature. *J. Atmos. Oceanic Technol.,* **5,** 197–205, doi:10.1175/1520-0426(1988)005<0197:TFERAV>2.0.CO;2.

Zrnić, D. S., G. Zhang, V. Melnikov, and J. Andric, 2010: Three-body scattering and hail size. *J. Appl. Meteor. Climatol.,* **49,** 687–700, doi:10.1175/2009JAMC2300.1.